

Antimicrobial Finish of Polyethersulfone Membranes: Sticking Photosensitizers-Like Marine Mussels Would Do

Anna Grafl, Alexander Müller, Annegret Preuß, Beate Röder, and Hans. G. Börner*

Biofouling is one of the most serious problems in membrane filtration systems for water treatment. An easily applicable antimicrobial finish of polyethersulfone (PES) filter membranes is shown by derivatizing an approved chlorin photosensitizer drug with adhesive *ortho*-catechol functionalities as known from L-3,4-dihydroxyphenylalanin (Dopa) residues of marine mussel glues. The chemical structure of the second-generation photosensitizer 5,10,15,20-tetrakis(3-hydroxyphenyl)chlorin (*m*-THPC) is modified by 2-iodoxybenzoic acid (IBX) oxidation, transforming the peripheric *meta*-phenols of *m*-THPC into *ortho*-catechols, and thus improving the adsorption properties of *m*-THPC derivatives onto PES material. Stable coatings are formed that preserve chlorin's capability to generate singlet oxygen under visible light illumination. The modification of one or two phenol groups out of the four *m*-THPC substituents leads to an optimum in the generation of active singlet oxygen, and thus the finish significantly reduces the bacterial growth of gram-negative *Escherichia coli* and gram-positive *Micrococcus luteus* on the PES membranes.

The global market of antimicrobial coatings^[4] is predicted to reach 11.6 billion USD by 2027 and various strategies have been investigated to prepare antimicrobial surfaces.^[5] For instance, surface deposition of quaternary ammonium compounds or antimicrobial peptides as well as topology design by lithography or attachment of carbon nanotubes results in antimicrobial material surfaces.^[6] Additionally, high surface area silver or copper as well as TiO₂ (nano)particles were successfully exploited.^[7] However, adverse effects are described depending on the concentration, size, and duration of exposure.^[8] Based on widespread use, environmental risks^[9] as well as the potential development of bacterial resistance^[10] might require the exploitation of alternative mechanisms of action. Functional organic molecules offer

1. Introduction


In times of globally fast spreading multiresistant microbes, antibacterial and microbial materials are of major importance.^[1] Particularly, antibacterial finishes of natural or synthetic yarns, wovens, and polymer membranes are urgently demanded as bacterial adhesion and biofilm formation on such material surfaces tend to be persistent and cause sincere problems concerning the product lifespan and health-related issues.^[2] Applications of antimicrobial materials are found in various areas, ranging from health care to fitness training and sports, to facade wall paints.^[3]

opportunities to produce environmentally friendly reactive oxygen species (ROS), which usually act confined and if required nonpermanent by using light as a trigger. For instance, porphyrins or chlorins are commonly established nontoxic photosensitizers to generate singlet oxygen ¹[O₂], upon visible light irradiation, which does not interfere with material integrity compared to harsh UV light.^[11] The mechanisms of ¹[O₂] production and its action on biosystems as well as solubilization and delivery of photosensitizer moieties have been explored intensively as these provide the underlying base for the potent photodynamic therapy (PDT).^[12] ¹[O₂] is considered to be a highly reactive species and oxidizes proteins or lipids that could induce apoptosis or eradication of bacterial growth.^[13] Singlet oxygen is proved to be effective against various gram-negative and gram-positive bacteria and can cope with severe multidrug-resistant isolates.^[14] Due to the limited lifetime of singlet oxygen, the antimicrobial efficacy is closely localized to the microenvironment of the photosensitizer-equipped surface and, e.g., environmentally friendly chlorins showed absence of toxicity in darkness.^[15] For instance, *meso*-tetra(4-carboxyphenyl)porphine (TCPP) was self-assembled with triaminoguanidinium chloride (TG) forming cationic TCPP-TG nanoparticles that inactivate bacteria growth under visible light irradiation.^[16]

Technical polymer membranes used in water filtration systems particularly demand retaining of sterile surfaces during consumer lifespan to reduce the risk of severe water contamination.^[17] To provide bacteria-free surfaces on such membranes, e.g., interval treatment based on biocide dosing, as well as physical or chemical cleaning procedures have been used.^[18] However, with the advent of low-energy light emitting diodes (LED),

A. Grafl, H. G. Börner
Laboratory for Organic Synthesis of Functional Systems
Department of Chemistry
Humboldt-Universität zu Berlin, 12489 Berlin, Germany
E-mail: h.boerner@hu-berlin.de

A. Müller, A. Preuß, B. Röder
Department of Photobiophysics
Humboldt-Universität zu Berlin
12489 Berlin, Germany

 The ORCID identification number(s) for the author(s) of this article can be found under <https://doi.org/10.1002/adem.202201279>.

© 2022 The Authors. Advanced Engineering Materials published by Wiley-VCH GmbH. This is an open access article under the terms of the Creative Commons Attribution-NonCommercial-NoDerivs License, which permits use and distribution in any medium, provided the original work is properly cited, the use is non-commercial and no modifications or adaptations are made.

DOI: 10.1002/adem.202201279

mechanisms of PDT were expanded to protect filtration membranes from biofouling by $^1\text{O}_2$ generation.^[19] Within the context of PDT, structure–activity relationships of photosensitizers were deeply investigated and several entities were described showing high $^1\text{O}_2$ production efficiency, excellent bioactivity, and low dark toxicity.^[20] Different means were explored to equip surfaces with photosensitizers. These strategies involved, for instance, 1) blending of PDT-active additives to the bulk material prior to membrane/yarn processing; or 2) postprocessing of fibers or membranes, e.g., by electron beam irradiation to covalently attach photosensitizers; 3) interfacial polymerization of functional monomers, as well as 4) layer-by-layer deposition to generate antimicrobial coatings.^[19,21] Recently, Ghiladi, Spontak, and coworkers described interesting approaches to deposit a porphyrin-based PDT additive on fiber materials and reported high antimicrobial activity with broadspectrum antibacterial potentials.^[21b,21c,22] However, the coating processes relied usually on reactive coadditives to covalently attach or embed the PDT additive as a coating on various material surfaces.^[23]

Here, we present the derivatization of the photosensitizer 5,10,15,20-tetrakis(3-hydroxyphenyl)-chlorin (*m*-THPC, **Scheme 1**) to which adhesive moieties were introduced for ease of deposition of a photoactive antimicrobial coating on material surfaces. Inspired by marine mussel adhesives^[24] and biomimetic mussel glue polymers^[25] that present L-Dopa as key residues for underwater adhesion onto various substrates, the phenolic substituents of *m*-THPC were oxidized to *ortho*-catechols. Catechol moieties are showing strong and robust adhesion in salt water solutions and proved interactions to various materials due to hydrogen bonding, metal ion coordination, as well as π - π or π -cation interactions.^[26] The coating behavior of the set of adhesively equipped *m*-THPC derivatives was studied on polyethersulfon (PES) microfiltration (MF) membranes as technically used water filters. The PES membranes show high mechanical strength, pronounced temperature tolerance, wide pH stability as well as pore sizes of 0.2 μm holding back plankton, algae, bacteria, and suspended solids.^[27] The membranes were coated with different *m*-THPC derivatives, possessing 1, 1&2, and 4 adhesive *ortho*-catechol functionalities, and the coating stabilities were investigated under static conditions. The $^1\text{O}_2$ production was

monitored by time-resolved near-infrared (NIR) luminescence and phototoxicity properties were tested on biofilm formation with *Escherichia coli* and *Micrococcus luteus*.

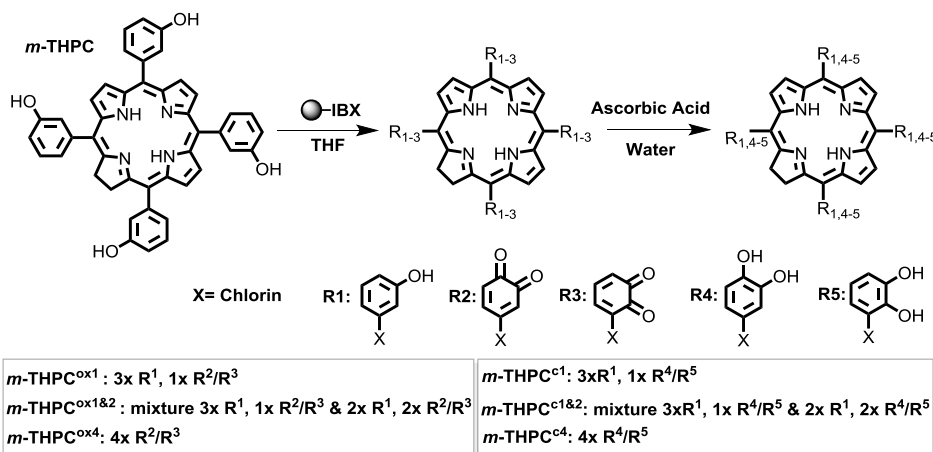
2. Results and Discussion

2.1. Synthesis of the Photosensitizer Library

The PDT sensitizer *m*-THPC (Scheme 1) appears to be most suited to be equipped with adhesive functionalities, as the chemical structure exhibits already four peripheral *meta*-phenol substituents, which could be transformed into catechol functionalities by oxidation. Moreover, *m*-THPC was clinically approved for photodynamic cancer therapy applications on head and neck carcinoma.^[28] The drug and respective formulations have been intensively investigated to improve applicability and barrier transport.^[29] *m*-THPC belongs to the second-generation photosensitizers and is known for a high singlet oxygen quantum yield, low toxicity in the dark, and insensitivity against environmental changes.

Oxidation of *ortho*-phenols to *ortho*-catechols can proceed either by enzymatic means via phenol oxidases such as tyrosinase-like enzymes or by 2-iodoxybenzoic acid (IBX), where established protocols can be adapted by using supported IBX for ease of purification.^[30]

A set of *m*-THPC derivatives was synthesized, differing in the number of catechol functionalities (Scheme 1). Chlorins featuring only one catechol moiety out of the four phenol substituents (*m*-THPC^{c1}) should less strongly bind to PES membranes, whereas the fully oxidized chlorins with four catechol groups (*m*-THPC^{c4}) should adsorb onto PES membranes with maximum of contacts possible. Despite the difficulties that originate from structural isomers, the chlorin derivative exhibiting two catechols was attempted (*m*-THPC^{c2}) as it might attach in an intermediate manner to PES surfaces. Dependent on the targeted degree of modification, different equivalents of supported IBX (S-IBX) were used. With respect to the *m*-phenol moieties of *m*-THPC, three, five, or twenty-four equivalents of S-IBX were added to a solution of *m*-THPC to obtain single, double, and fully oxidized products, respectively. After the oxidation, S-IBX was



Scheme 1. Illustration of the synthesis of *m*-THPC derivatives yielding *m*-THPC^{c1}, *m*-THPC^{c1&2}, and *m*-THPC^{c4} with enhanced adhesive properties.

filtered off and the supernatant was purified using flash chromatography to separate unmodified *m*-THPC starting material from the oxidation products. It should be noted that IBX oxidizes phenols in a two-step reaction to *ortho*-quinones (*m*-THPC^{ox}), which have compared to the catechols a strongly reduced interaction capability, and thus make the use of chromatography feasible. While purification of *m*-THPC^{ox1} and *m*-THPC^{ox2} were required, the high excess of S-IBX utilized during the synthesis of *m*-THPC^{ox4} pushed the reaction to completion and makes chromatographic workup obsolete. Due to the different structural isomers, the oxidation product *m*-THPC^{ox2} could not be isolated as a single compound. Therefore, the intermediately oxidized *m*-THPC^{ox1&2} was used in this proof of principle study as a mixed batch, showing 15% of *m*-THPC^{ox2} and 85% of *m*-THPC^{ox1} as determined by UPLC-MS (Figure S2, Supporting Information).

After workup and purification, the oxidized *m*-THPC derivatives were reduced by ascorbic acid to obtain the desired catechol analogues *m*-THPC^{c1}, *m*-THPC^{c1&2}, and *m*-THPC^{c4}. The modified chlorins were characterized with UPLC-ESI-MS, as well as by NMR, UV/vis, and fluorescence spectroscopy (Figure S1–S5, Supporting Information). Taking into account, the asymmetry in the chlorin core of *m*-THPC that is caused by one hydrogenated pyrrole ring, and considering moreover, that IBX oxidation can lead to 1,2- or 2,3-quinones,^[31] the formation of four different *m*-THPC^{c1}, fourteen different *m*-THPC^{c2}, and ten different *m*-THPC^{c4} isomers can be expected. This was reflected in the UPLC chromatograms, showing several isomers that elude at slightly different retention times, but exhibit the same molar masses as shown by ESI-MS detection (Figure S2, Supporting Information). It should be noted that UPLC was not able to separate all expected isomers, as some of which have rather a low propensity to be formed and rather similar elution properties (Figure S2 and S3, Supporting Information). The precise analysis of isomer compositions would require the synthesis of chlorin standards by a stepwise ring condensation route, which would be interesting, but beyond the scope of this application-oriented study.

2.2. Spectroscopic Properties of the Chlorin Derivatives

The UV/vis and fluorescence spectroscopy analyses of the *m*-THPC derivatives provide insight into changes in the electronic structure and photophysical properties of the photosensitizer (Figure S4 and S5, Supporting Information). UV/vis spectra show in all cases the typical $Q_{y(0 \rightarrow 0)}$ -band for chlorins that occurs for *m*-THPC at 651.0 nm. This band was only marginally blue-shifted for *m*-THPC^{c1}, *m*-THPC^{c1&2}, and *m*-THPC^{c4} to be observed at 645.3, 644.8, and 650.5 nm, respectively. Moreover, the Soret band occurs for *m*-THPC at 420.5 nm and was found also to be only slightly blue shifted to 419.5 nm for the derivatives *m*-THPC^{c4} and *m*-THPC^{c1&2} as well as to 418.0 nm for *m*-THPC^{c1}. The Soret band as well as the vibronic Q_y - and Q_x -bands originate primarily from the electron dipole movements that enable π - π^* transitions. The minor shifts of the absorption maxima suggest the π -system, which constitutes the chlorin core structure, to be not dramatically affected by the additional hydroxyl substituents.^[32]

The fluorescence spectroscopy of the original photosensitizer and its derivatives revealed more pronounced effects. All compounds show in ethanol a fluorescence maximum at 652 nm on excitation at 418 nm (Figure S4, Supporting Information). However, the fluorescence intensity of these maxima decreased systematically with increasing number of hydroxyl substituents. Where *m*-THPC^{c1} reached 64% of the *m*-THPC fluorescence intensity, *m*-THPC^{c1&2} reached 60%, and *m*-THPC^{c4} showed only 40%. These observations were consistent with Bonett et al., reporting that within the photobleaching process of *m*-THPC similar photoproducts as the *m*-THPC^{ox} are produced, causing a decrease in the fluorescence intensity.^[33] The fluorescence spectroscopy analysis confirmed the chlorin π -system to be not dramatically altered by the introduced catechol moieties. However, decreased fluorescence intensities of the *m*-THPC^{ox} derivatives are evident in increasing degree of derivatization. This might indicate higher propensities for intersystem crossing, nonradiational competing processes, or catechol quenching effects to get more prominent.

2.3. Finish Deposition onto PES Membranes and Coating Stability

The set of *m*-THPC^{ox} derivatives was studied to be noncovalently attached to surfaces of PES membranes. To correlate the coating behavior with the type of photosensitizer functionalization, model PES membranes were used in static experiments, avoiding the complex setting and flow-shear conditions of applied water filtration PES membrane systems. However, the coating of model membranes under static conditions revealed differences in both the adsorption properties onto PES and the coating stabilities. For this purpose, *m*-THPC and the modified photosensitizers *m*-THPC^{c1,1&2,4} were dissolved each in ethanol. The 1 cm² PES membranes were weighed for normalization purposes and incubated for 1 h under gentle shaking with stock solutions of different chlorin concentrations (0.075, 0.15, 0.25, and 0.5 mg *m*-THPC^{ox} per mL). After removal of the PES membranes from the incubation bath, the coated membranes were washed with aqueous solution of ascorbic acid to avoid air oxidation of the catechols. Subsequently, elution experiments were performed to investigate the coating stability by washing the coated PES membranes with different solvents. The solvation strength was progressively increased from 50% aqueous ethanol, to pure ethanol to remove weakly bound photosensitizers, while strongly adsorbed chlorins should remain anchored. After each washing step, the absorbance of the rinsing solutions at the $Q_{y(0 \rightarrow 0)}$ -band absorption maxima was measured to determine the chlorin concentration based on calibration curves (Figure S7, Supporting Information). The residual amount of chlorins that strongly binds onto the PES membranes and survived the different washing steps, was accessible by dissolving the coated membranes in dimethyl sulfoxide (DMSO) and analyzing the chlorin concentration via UV/vis spectroscopy.

For all compounds, it was found that the higher the incubation concentrations have been, the more chlorin was deposited onto PES membranes (Figure 1a). As expected, *m*-THPC^{c4} deposited in the range of accessed incubation concentrations always with the highest amounts onto PES. Interestingly, up to

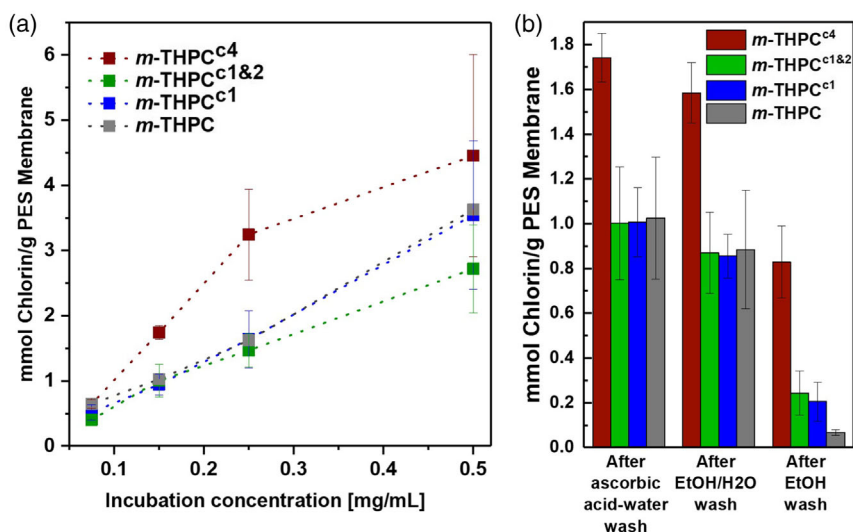


Figure 1. Incubation and elution studies of the set of chlorin derivatives on PES membranes (mean \pm standard error). a) Concentration-dependent deposition of chlorins during incubation of PES membranes with different stock solutions deposited amounts after fixation with ascorbic acid and intense water washes and b) stability of PES membrane coatings showing material losses of different chlorin derivatives by washing steps with EtOH/water (50 vol %), EtOH, and finally eluted remaining chlorins by DMSO. (Conditions: Incubation: 1 h, r.t., 1 mL incubation solution, 1 cm² PES membrane (about 6.5 mg), Elution: washing with 1 mL, 20 min. shaking; experiments were performed at least in triplicates, lines in (a) are to guide the eye).

concentrations of about 0.25 mg mL⁻¹, the derivatives *m*-THPC^{c1} and *m*-THPC^{c1&2} as well as the *m*-THPC showed within the error of the experiment rather similar amounts deposited. The *m*-THPC^{c4} proved at incubation concentration of 0.25 mg mL⁻¹ an up to 215% higher material deposition. Apparently, above 0.25 mg mL⁻¹, the deposition of *m*-THPC^{c4} starts to run into saturation, while the other chlorin derivatives continue to follow an almost linear relation. The incubation step of PES membranes with chlorin stock solutions of 0.15 mg mL⁻¹ yields suitable coatings and the stability of those was more closely investigated in elution experiments (Figure 1b).

PES membrane incubation with *m*-THPC^{cx} stock solutions of 0.15 mg mL⁻¹ lead to *m*-THPC^{c4} to coatings with 175% higher deposited amounts, compared to the other chlorins that reach all the same amount of material deposition. All coatings were fully stable against rinsing with water or sea water model solutions of 599 mmol NaCl. Moreover, the coatings proved decent stability against washing with 50% EtOH/H₂O, showing only 9–15% material wash-off from the coated PES membranes. Apparently, under the conditions of ethanol/water washing steps, no differentiation between the interactions of the different chlorin derivatives and the PES was obvious. The ethanol washing step results in larger differences between the chlorins, proving significant effects of the number of anchor sides on coating stability. While *m*-THPC^{c4} preserved 52% material as stable coating, only 7% of the *m*-THPC coating could not be washed off. As expected, *m*-THPC^{c1} and *m*-THPC^{c1&2} exhibit quite similar characteristics, where 24% and 28% of the coating materials could not be eluted and retained as stable coatings. Obviously, ethanol is a solvent able to overcome the weaker interactions of chlorins with the PES surface, and equipping *m*-THPC with additional anchor groups has a significant effect on coating stability. With respect to potential applications, 10 g of *m*-THPC^{c1} would

enable to coat about 1800 m² of PES membranes (Table S3, Supporting Information). Most importantly, all different coatings were not interfering dramatically with the capability of the filter membranes to let water pass. This was demonstrated by an initial flux test under unpressurized conditions that show no significant reduction of water flow through the PES membranes prior and after chlorin coating (Table S4, Supporting Information).

The comparison between the different chlorin coatings obtained by incubation of the PES membranes with 0.15 mg mL⁻¹ chlorin solutions showed that *m*-THPC^{c4} reached about 12 \times higher material deposition than *m*-THPC, as well as 3.4 \times and 4 \times higher than *m*-THPC^{c1&2} and *m*-THPC^{c1}, respectively. With the knowledge of the membrane loadings, a rough estimation of the coverage after ethanol washes can be made, taking the specific surface area of the PES membranes of 7 \pm 1 m² g⁻¹ into account (N₂ adsorption analysis with BET-model, Table S1, Supporting Information). The molecular dimensions and idealized packing of the chlorins on the surfaces were estimated based on low-level computational models applying geometry optimization (cf. Table S2, Supporting Information). The discotic structure and the reduced conformational flexibility of the chlorin molecules enabled to approximate a planar molecule with quadratic shape (Figure 2a). The simple model reveals the length of the edges, the Connolly solvent excluded volume (CSEV), and the projected molecule area of the discotic structure (Table S2, Supporting Information). While the latter defines the interface that is ideally covered in case of the chlorin anchors only “plain-on” flat onto the substrate, the former enables estimation of the required interface if the chlorin anchors “edge-on” and stand perpendicular to the substrate.

Considering a “plain-on” adsorption of chlorins (Figure 2b,c) and ignoring demands of solvation layers, the required area for chlorins in relation to a single monolayer would be larger by a

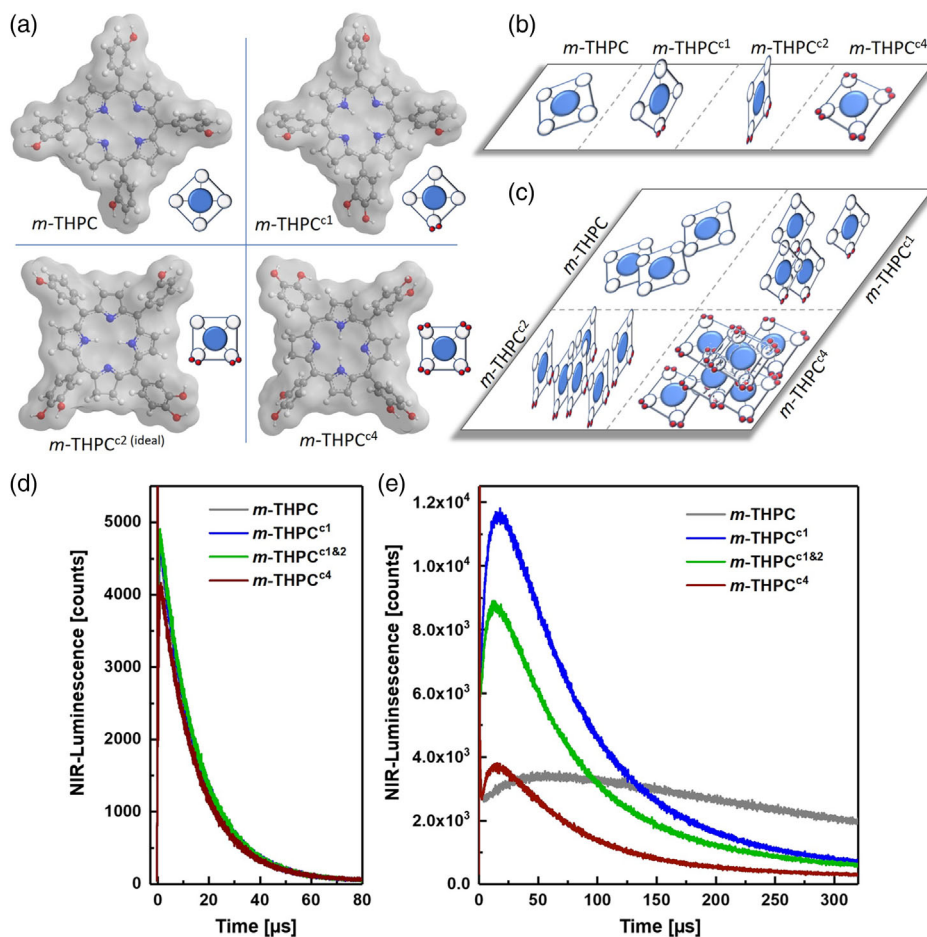


Figure 2. Idealized illustration of the molecular structures of chlorins m -THPC, m -THPC^{c1}, m -THPC^{c2(syn-ideal)}, and m -THPC^{c4} indicating the introduced adhesion points that dominate the surface contacts a) and define positioning b) and packing in coatings c). Singlet oxygen production of the different m -THPC derivatives by time-resolved NIR-luminescence measurements under homogeneous solution conditions in ethanol d) and heterogeneous conditions from water-soaked coated PES membranes e). (Conditions: (c,d) monitoring at 1270 nm (FWHM, λ_{ex} = 405 nm, r.t., absorbance = 0.08 ± 0.01). (e) Scanning a 6×6 pixel raster per 1 mm increment with measurement times of 10 s pixel⁻¹ and summation over all 36 pixels. Membranes were loaded with photosensitizers (incubation concentration: 0.15 mg mL⁻¹), washed with ethanol, and soaked in water).

factor of about 10 for m -THPC, 25 for m -THPC^{c1}, 30 for m -THPC^{c1&2}, and even 120 for m -THPC^{c4} (Table S3, Supporting Information). For the “edge-on” packing model (Figure 2b,c, Supporting Information), the covered area required to form a monolayer on the PES surface is larger by a factor of 3 for m -THPC, 7 for m -THPC^{c1}, 9 for m -THPC^{c1&2}, and 34 for m -THPC^{c4} (Table S3, Supporting Information). Considering the rough assumptions underlying both models, as well as the error of the BET method operating not in the most accurate surface area regime, a sufficient coverage of the PES membranes can be assumed. The fact that m -THPC can be largely washed off by ethanol suggests the importance of the catechol groups as dominating anchor moieties for the m -THPC^{cx} derivatives. Thus, it seems to be straightforward to speculate that the symmetric m -THPC^{c4} is probably packing flat in multilayers, while the m -THPC^{c1} and an idealized m -THPC^{c2} would pack upright “corner-on” or “edge-on” with less prominent tendencies to form multilayers.

2.4. Photoactivity of the Chlorins and Singlet Oxygen Production

It should be noted that the different modes of chlorin packing within PES coatings might affect ¹[O₂] production capabilities. However, before investigating the photosensitizer functions in the anchored states, initial solution experiments analyzed the different chlorin derivatives, independently of packing and surface effects. Under comparable photophysical boundary conditions, the singlet oxygen production can be monitored by time-resolved near-infrared (NIR)-luminescence at 1270 ± 15 nm using an excitation wavelength of 405 nm.^[19] All chlorins were fully-insoluble in water, but readily soluble in ethanol and proved under these homogeneous conditions to produce ¹[O₂] effectively (Figure 2d). The nonmodified m -THPC as well as both m -THPC^{c1} and m -THPC^{c1&2} reached practically the same NIR-luminescence intensity and radiation decay proceeds in a corresponding manner. Even the highly derivatized m -THPC^{c4} yielded

about 90% of the NIR-luminescence maximum of *m*-THPC and radiation decay occurs similarly. Thus, equipping *m*-THPC with mussel-inspired adhesive functionalities does not dramatically influence the sensitive electronic properties of the chlorin core and consequentially the photosensitizer functions were retained.

While solution experiments were promising, the ultimate proof of preserving the photosensitizer function in the *m*-THPC derivatives has to consider the anchored chlorin states. Sensitizer-loaded membranes were analyzed by time-resolved NIR-luminescence scanning. Therefore, the chlorin-coated membranes were carefully washed with ethanol and after equilibration in water, the luminescence of the water-soaked membranes was measured by scanning an area covering 6×6 pixels with pixel distances of 1 mm and scanning laser spot sizes of about $d = 100 \mu\text{m}$. The resulting NIR-luminescence intensities were cumulated in overall signals, representative of the respective photosensitizer activities within the coatings.

The analysis confirmed distinguishable differences in NIR-luminescence, depending on the photosensitizer (Figure 2b). All derivatives *m*-THPC^{c1}, *m*-THPC^{c1&2}, and *m*-THPC^{c4} exhibited a distinct signal maximum at 14–20 μs and a rapid decay afterward. In contrast to that, the *m*-THPC coatings exhibited a lower maximum at 46 μs and a longer decay time. The time of the luminescence maxima correlates with the lifetime of the triplet state and/or the singlet oxygen state, which are significantly higher in the coating than in the solution. The retarded and low maximum of *m*-THPC might be explained by a denser aggregation of *m*-THPC in the coating layer, which is consistent with a model, describing the aggregation of *m*-THPC in the biological environment.^[20,34]

Interestingly, the *m*-THPC^{c1} coating reached by far the highest maximum of luminescence intensities compared to all derivatives. The luminescence of *m*-THPC^{c1&2} and *m*-THPC^{c4} exhibited 74% and 33% of that of *m*-THPC^{c1}. *m*-THPC^{c4} meets a similar range observed for the coating of *m*-THPC. Surprisingly, the coating of *m*-THPC^{c4}, which has the highest mass deposition after ethanol washing in the incubation and elution experiments, and the coating of *m*-THPC with the lowest amount of stably deposited chlorin have similar luminescence intensity maxima. It appears to be even more noteworthy that a coating of *m*-THPC^{c1} having only 25% of the deposited chlorin compared to *m*-THPC^{c4}, reached 200% higher luminescence intensity maximum, and thus performs significantly better in ¹[O₂] generation. Taking into account that all compounds show rather similar ¹[O₂] production capabilities in homogeneous solutions, the photosensitizer activity in the coatings depends primarily not on the deposited amount at the PES membrane surface, but is dramatically influenced by factors such as molecule packing and orientation. This finding was expected, as these parameters define not only the propensity of self-quenching, but also the diffusion of oxygen into the chlorin coatings.

The differences in the NIR-luminescence curves suggest that the microenvironment of *m*-THPC^{cx} is rather dissimilar between the coated and the homogenous solution states. The packing argument appears for the coating to be rather important. Obviously, the mussel-inspired adhesive catechols are one of the dominating sites for defining anchoring, deposition, and orientation of *m*-THPC^{cx} onto the PES surfaces. In Figure 2,

idealized attachment and packing modes for the different chlorin structures were anticipated. Due to the discotic molecular shape and the symmetry, *m*-THPC and *m*-THPC^{c4} attach most likely similar in a preferentially “face-on” contact onto the surface. Such contact is less preferred, as surface-induced quenching of both the excited chlorin state and/or the generated ¹[O₂] species might occur to jeopardize the photosensitizing process.^[35] The *m*-THPC^{c4} has four catechol anchor groups and attaches most effectively to PES substrates. However, intermolecular catechol interactions might be expectable to stabilize multilayers. Those would additionally contribute strongly to self-quenching as described for *m*-THPC,^[35] which is consistent with the low singlet oxygen production rates found in *m*-THPC^{c4} coatings. In contrast to *m*-THPC^{c4}, *m*-THPC^{c1} is expected to anchor via one corner, depositing less amounts and providing the sensitizer with higher flexibility. Apparently, such mode of attachment reduces self-quenching and improves accessibility for triplet oxygen species that would rationalize the highest ¹[O₂] production rates found for *m*-THPC^{c1} coatings. The *m*-THPC^{c1&2} mixture might include isomers making “edge-on” attachment feasible. This results in more stable anchoring, but seems to be not ideal as more densely packed photosensitizers might enhance self-quenching, as well as could reduce diffusion of both oxygen into and singlet oxygen out of the coating.^[36]

2.5. Bacterial Growth Inhibition and Phototoxicity

The efficient generation of singlet oxygen within the *m*-THPC^{cx} finishes of PES membranes is promising. However, the reactive oxygen species require ultimately to reach the microbial organisms to induce antimicrobial properties. Surface topographies in the microstructure range might have relevance to inhibit bacterial settlement and physically prevent biofilm formation.^[37] Thus, the structure of the PES membranes before and after coating was characterized by scanning electron microscopy (Figure S8, Supporting Information), proving no indications for dramatic topology differences. The PES membranes show in both cases similar surfaces and primary pores in the range of 10–20 μm , indicating that no clogging of the primary membrane structure by chlorin coatings was evident. This is consistent with an initial flux test, confirming within the error of the experiment in all cases no dramatic alternation of water flow after chlorin coating, even for those membranes coated densely with *m*-THPC^{c4} (Table S4, Supporting Information). Contact angle analysis of the set of membranes could not be reliably interpreted as surface topology superimpose with polarity, which is a commonly found effect for microstructured surfaces.^[38]

It should be noted that the biofilm formation on membrane systems depends strongly on several factors such as material surface chemistry, membrane roughness, porosity, and shear forces under flow conditions. To reach comparability of the phototoxic activities, the model PES membranes coated with different photosensitizer derivatives were microbiologically analyzed under static conditions. Avoiding the complexity of conditions closer to applied technical water filter systems ensures that the analyzed antimicrobial profiles were independent of minor differences in flow-through conditions. An initial nonquantitative study evaluated the antimicrobial activity of a chlorin coating in a

photobiophysical setting on gram-positive *M. luteus* bacteria. The phototoxicity of PES membranes coated with *m*-THPC^{c1&2} as well as either noncoated or *m*-THPC-coated controls was studied initially. The membranes were each cut into quarters and 50 μL (10^8 cells mL^{-1}) of *M. luteus* was seeded onto each part. While one quarter was kept in the dark to determine dark toxicity, the others were irradiated with white LED light of 11 mW cm^{-2} intensity. As anticipated *M. luteus* growth was strongly suppressed on *m*-THPC^{c1&2}-coated PES membranes after irradiation, where only minor stains have been visible (Figure 3a). Compared to that, bacterial growth was apparent on all nonirradiated controls, including *m*-THPC^{c1&2} coatings as well as on irradiated *m*-THPC coatings.

Quantitative phototoxicity studies were carried out with gram-negative *E. coli* which constitutes relevant bacterial models for water filtration applications. The inhibition of bacterial growth was investigated on coated PES membranes, exhibiting *m*-THPC, *m*-THPC^{c1}, *m*-THPC^{c1&2}, or *m*-THPC^{c4} coatings as well as on the noncoated references. The coated membranes

were roughly washed first with ethanol and water followed by equilibration in water. Afterward, the membranes were cut into two parts and each was inoculated with 100 μL of an *E. coli* suspension (10^8 cells mL^{-1}). While one sample was irradiated with white LED light of 11 mW cm^{-2} intensity, the corresponding control sample was kept in the dark. After the irradiation, the membranes were washed and gently shaken for 1 h in PBS buffer (pH 7.4) to elute the bacteria. 20 μL aliquots were taken and diluted 1:10, 1:100, 1:1000, up to 1:10 000 to be seeded on agar plates and incubated overnight at 28 $^{\circ}\text{C}$. The colony-forming units (CFU) were counted and the total quantities of CFU were calculated (Figure 3b and Table S5, Supporting Information).

The phototoxicity study indicated visible antibacterial activity on gram-negative *E. coli* growth for both irradiated *m*-THPC^{c1}- and *m*-THPC^{c1&2}-coated membranes, if compared to the references. The *m*-THPC^{c1} and *m*-THPC^{c1&2} coatings were able to reduce bacterial growth under irradiation by 3-4 \log_{10} units. Thus, up to 99.99% of the bacterial growth was suppressed, which meets the specification to be categorized as biologically relevant and antimicrobial activity.^[39] It seems to be remarkable that 33% of the *m*-THPC^{c1} and 21% of the *m*-THPC^{c1&2}-coated PES membranes showed no bacteria growth at all (Table S5, Supporting Information). Instead, the *m*-THPC^{c4}- and *m*-THPC-coated PES membranes decreased the bacterial growth less dramatically. The two-sample *t*-test showed significant differences between nonirradiated and irradiated pairs for all chlorine coatings as well as for the nonmodified membranes (Table S6, Supporting Information). The white light irradiation in the photobiophysical setting leads to a minor reduction of *E. coli* growth as found in the noncoated references, if bacterial growth in the dark is compared to that under irradiation. This effect is known,^[40] but comparing the intensity of growth reduction to the phototoxicity found in coated PES membranes, proved high activity of the well-performing photosensitizers *m*-THPC^{c1} and *m*-THPC^{c1&2}.

Comparing the antimicrobial activity of the best performing *m*-THPC^{c1} PES coating with other literature-described surface modification systems, categorizes the *m*-THPC^{c1} finish as well balanced between straightforward to be applied and sufficiently active for potential applications. For instance, electron beam fixation of the polycationic photosensitizer TMPyP, resulted in coated membranes that show phototoxicity of 6 \log_{10} units for *E. coli*.^[19] The porphyrin photosensitizer ZnTMPyP⁴⁺ tetrachloride required codeposition and crosslinking of a UV-curable poly(vinyl alcohol) derivative. The resulting coatings on polymer microfibers reduced exceptionally well the growth of gram-positive *Staphylococcus aureus* by $>6 \log_{10}$ units and by $<3 \log_{10}$ units the growth of *E. coli*.^[22] A similar order of magnitude was achieved for the incorporation of silver nanoparticles into cotton fibers, reducing the growth of *S. aureus* by 3 \log_{10} units,^[41] antimicrobial ceragenin peptides immobilized on hydrogel contact lenses reduce the growth of *P. aeruginosa* (gram negative) and *S. aureus* by 3 \log_{10} units,^[42] mixed ureidopyrimidinone-based supramolecular polymers with antimicrobial peptides lead to a growth reduction of *E. coli* by $\leq 3 \log_{10}$ units,^[43] as well as a commercially available product composed of polyacrylate-based copolymer material reached growth reduction of 4–6 \log_{10} units for *S. aureus*, *K. pneumoniae* (gram-negative), *P. aeruginosa*, and *S. epidermis* (gram-positive).^[44]

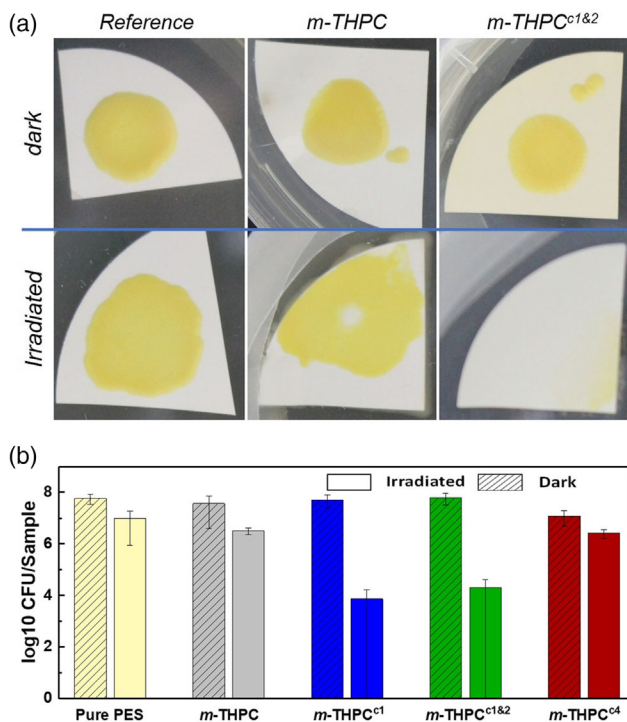


Figure 3. Antimicrobial activity studies on *Micrococcus luteus* a) and *E. coli* b) determining the phototoxicity of photosensitizer-coated PES membranes under white LED light irradiation and nonirradiated controls for dark toxicity (mean \pm standard error, $n = x$). Qualitative test on inhibition of *M. luteus* growth ($n = 6$) (a) and quantification of colony-forming units (CFU) to analyze photoinduced growth inhibition of *E. coli* ($n = 16$ –54) (b). (Conditions: Membranes were inoculated with bacterial suspension (50 μL (10^8 cells mL^{-1}), *M. luteus*, (a) and 100 μL (10^8 cells mL^{-1}), *E. coli* (b)); parts of the membranes were irradiated with 11 mW cm^{-2} white light LED for 1 h and the control parts were kept in the dark. CFU quantification includes *t*-test results and mark significance). A two-sample *t*-test, with one- and two-tailed *p*-values was done for all membranes (Table S5, Supporting Information).

Beyond the promising activity of the *m*-THPC^{c1} finish on PES microfiltration membranes and the proven singlet oxygen luminescence of water-soaked membranes, there remains room for engineering and technical optimization, to develop the finish toward usability in applied water filtration modules. Within those dynamic systems sheer flow, pressure drop profiles, salt concentration gradients in hand with antibacterial activity, and dead bacteria clearance by sheer flow will critically determine the antimicrobial time profiles and biofilm formation kinetics.

3. Conclusion

The second-generation photosensitizer drug *m*-THPC which is partially FDA approved for photodynamic cancer therapy was chemically modified by introducing *ortho*-catechol moieties onto peripheric *meta*-phenol groups. As known from 1-3,4-dihydroxyphenylalanine (Dopa) residues of the mussel adhesive system, catechols enhanced binding capabilities of *m*-THPC to noncovalently attach to material surfaces, e.g., PES filter membranes, and are expected to exhibit excellent robustness of adhesion properties in many aqueous solutions. A set of *m*-THPC derivatives exhibiting one, and four, as well as a mixture of one-two catechols (*m*-THPC^{c1}, *m*-THPC^{c4}, *m*-THPC^{c1&2}), were accessed by straightforward oxidation with resin supported 2-iodoxybenzoic acid (S-IBX). Depending on the number of introduced catechols the chlorin derivatives bind differently to PES membranes and widely tolerate in contrast to the nonderivatized *m*-THPC stronger washing conditions with ethanol. The amounts of photosensitizers that deposit on PES membranes as stable coatings, increase the number of catechol moieties present in the *m*-THPC derivative. However, not the highest loadings show the maximum singlet oxygen production and the most effective antimicrobial phototoxicity. Unexpectedly, *m*-THPC^{c1} and *m*-THPC^{c1&2} provide an optimum, proving the most promising antimicrobial coatings on PES membranes against highly relevant gram-negative *E. coli* and gram-positive *M. luteus* bacteria. In comparison, *m*-THPC^{c1} forms finish with 75% less materials compared to *m*-THPC^{c4}, but NIR-luminescence scanning shows 200% higher ¹[O₂] production that leads to 3.9 log₁₀ units reduction of *E. coli* growth. Obviously, densely packed *m*-THPC^{c4} multilayer coatings promote self-quenching that limits the effectivity of the photosensitizer. The introduced coating strategy that exploits adhesion mechanisms from marine mussels to anchor and position photosensitizers onto membrane surfaces, enables ease of processability and could be in-line with established fiber finish processes. Antibacterial-equipped membranes in combination with low-power LED vis light sources might effectively extend filter systems consumer live-span and prevent biofouling in water purification systems such as reversed osmosis, as well as nano-, ultra-, and microfiltrations. The implementation of photosensitizer coatings seems to be straightforward for hollow-fiber membrane modules as they float in clean water tanks, and thus are easily accessible for LED vis light irradiation. Certainly, *m*-THPC is a compound of high value, but the study proved that the controlled anchoring of a photosensitizer is an important factor for reducing active additive use and optimizing the antibacterial efficacy of coatings. However, the concept might be further translated to other

photosensitizer classes, which might be less robust compared to *m*-THPC and more cost-effective, to improve applicability.

4. Experimental Section

Materials: The following materials were obtained from commercial suppliers and used as received. PBS Buffer (Endotoxin-Free Dulbecco's PBS), Agar-agar, PES membranes (Millipore Express PLUS, 0.22 μm pore size, 47 mm diameter, thickness ≥160 and ≤185 μm), and microbiological culture media (yeast extract, tryptone, and sodium chloride) were obtained from Merck Millipore. Supported IBX on polystyrene (S-IBX, loading 1.23 mmol g⁻¹) was purchased from Novabiochem, acetonitrile (HPLC-MS grade), ethanol absolute (>99.7%), and tetrahydrofuran (THF) were obtained from VWR chemicals. *m*-THPC (M. Senge (Trinity College Dublin)), L-(+)-ascorbic acid (>99%, Carl Roth GmbH), and DMSO (>99%; Fisher Scientific) were used as received. Ethyl acetate, dichloromethane (DCM), and methanol were received from VWR chemicals and distilled prior to use. Aqueous solutions were prepared with ultra-pure water from a Laborstar SG Water system.

Synthesis of *m*-THPC^{c1} and *m*-THPC^{c1&2}: *m*-THPC (0.103 mmol, 70 mg) was solubilized in 10 mL of THF and depending on the targeted degree of functionalization 3 eq. or 5 eq. (251 mg, 0.309 mmol or 419 mg, and 0.515 mmol) supported S-IBX (1.23 mmol g⁻¹) was added. The reaction mixture was stirred for 12 h at room temperature and in the dark. The resin was removed by filtration and washed with THF. The reaction mixture was brought onto HYDRO-MATRIX for further purification by flash chromatography (DCM: MeOH, 95:5). After that *m*-THPC^{ox1} was solubilized in 3 mL of THF and was reduced by 4 eq. of ascorbic acid (72.6 mg, 0.412 mmol) in 10 mL of water and stirred for 1 h. An aqueous extraction with ethyl acetate was performed to remove the ascorbic acid. The solvent was distilled off under reduced pressure yielding 4.7 mg (0.0063 mmol, 6%) of pure *m*-THPC^{c1}. The low-yield results from reaction conditions to prevent overoxidation by targeting only 10% conversion, leaving the rest nonoxidized *m*-THPC. The yield of *m*-THPC^{c1&2} was 5.7 mg (0.008 mmol, 8%).

m-THPC^{c1}: ¹H NMR: (300 MHz, Aceton-d₆, δ in ppm): 1.84 (s, 2H, N-H), 4.14 (s, 2H, H_β), 4.43 (s, 2H, H_β), 7.26 (m, 5H, Ar-H), 7.58 (m, 10H, Ar-H), 8.41 (m, 2H, H_β), 8.52 (s, 2H, H_β), 8.75 (m, 2H, H_β). ESI-QMS: m/z calculated: [M + H]⁺ = 697.24; found: [M + H]⁺ = 697.30. FT-IR (ν(cm⁻¹)): 3290 (w), 2987 (m), 2883 (s), 2360 (w), 1633 (w), 1541, 1467, 1342 (m), 1280 (w), 1234 (w), 1147 (w), 1103 (vs), 1060 (s), 958 (w), 964 (w), 840 (w).

m-THPC^{c1&2}: ¹H NMR: (300 MHz, DMSO-d₆, δ in ppm): 1.67 (s, 2H, N-H), 4.14 (m, 4H, H_β), 7.0–7.62 (m, ≈15H, Ar-H), 8.21–8.82 (m, 6H, H_β), 9.0–9.8 (m, ca 5H, OH). ESI-QMS: m/z calculated: [M + H]⁺ = 697.24; found: [M + H]⁺ = 697.34. ESI-QMS: m/z calculated: [M + H]⁺ = 713.23; found: [M + H]⁺ = 713.29. FT-IR (ν(cm⁻¹)): 3290 (w), 2987 (m), 2883 (s), 2360 (w), 1633 (w), 1541, 1467, 1342 (m), 1280 (w), 1234 (w), 1147 (w), 1103 (vs), 1060 (s), 958 (w), 964 (w), 840 (w).

Synthesis of *m*-THPC^{c4}: *m*-THPC (0.03 mmol, 20 mg) was solubilized in 10 mL of THF and 24 eq. (0.720 mmol, 585 mg) supported S-IBX (1.23 mmol g⁻¹) were added. The reaction mixture was stirred in the dark for 12 h at room temperature. The resin was removed by filtration and *m*-THPC^{ox4} was reduced by the addition of 12 eq. (0.360 mmol, 63.4 mg) of ascorbic acid in 10 mL of water to the photosensitizer in THF. After stirring the reaction mixture for 1 h, the ascorbic acid was removed by aqueous extraction with ethyl acetate. The solvent was distilled off under reduced pressure yielding 15.6 mg (0.021 mmol, 71%) of *m*-THPC^{c4}.

¹H NMR: (300 MHz, DMSO-d₆, δ in ppm): 1.61 (m, 2H, N-H), 4.10 (m, 4H, H_β), 7.0–7.5 (m, 12H, Ar-H), 8.14–8.51 (m, 6H, H_β), 8.51–9.7 (m, 6H, OH). ESI-QMS: m/z calculated: [M + H]⁺ = 745.22; found: [M + H]⁺ = 745.27. FT-IR (ν(cm⁻¹)): 3290 (w), 2987 (m), 2883 (s), 2360 (w), 1633 (w), 1541, 1467, 1342 (m), 1280 (w), 1234 (w), 1147 (w), 1103 (vs), 1060 (s), 958 (w), 964 (w), 840 (w).

Coating Procedure of PES Membranes: The chlorins (*m*-THPC, *m*-THPC^{c1}, *m*-THPC^{c1&2}, and *m*-THPC^{c4}) were dissolved in different

concentrations (0.075, 0.15, 0.25, and 0.5 mg mL⁻¹) in ethanol. The complete membranes were incubated in 15 mL of the chlorin solution by shaking for 1 h. A 1 × 1 cm piece of the membrane was incubated in 1 mL of the chlorin solution. After removal from the incubation bath, the membranes were washed with aqueous solution of ascorbic acid (10 mg mL⁻¹) to prevent air oxidation of catechols and subsequently with water to remove excess ascorbic acid. The membrane was washed with 1 or 15 mL of a 50:50 mixture of water:ethanol, followed by washing with 1 or 15 mL of pure ethanol. For biotesting, the membranes were washed with water and equilibrated for 1 h in water prior to the application.

Phototoxicity: *M. luteus* growth inhibition tests were performed as a preliminary study for the qualitative evaluation of the phototoxicity of the coated membranes. *M. luteus* (wild type) was isolated from an airborne microbial sample on LB-agar. The membranes were cut in quarters, inoculated with 50 µL of a *M. luteus* suspension (10⁸ cells mL⁻¹), and irradiated with 11 mW cm⁻² (white light LED) for 1 h. The control membranes were parallel inoculated and kept in the dark. After this treatment, all samples were incubated in the dark for 2 days and then photographed for evaluation. For each batch, six samples were tested.

The *E. coli* (ATCC 25 922) growth inhibition tests were performed to quantify the phototoxicity of the coated membranes. The membranes were cut in halves, inoculated with 100 µL of an *E. coli* suspension (10⁸ cells mL⁻¹), and irradiated with 11 mW cm⁻² (white light LED) for 1 h. The control membranes were parallel inoculated and kept in the dark. After the incubation and irradiation, the samples were washed and shaken in 10 mL PBS buffer for 1 h. After that different dilutions were made from each sample (1:10, 1:100, 1:1000, 1:10 000). From every dilution, 8 times 20 µL were pipetted to agar plates. The agar plates were incubated overnight at 28 °C. Then the colony forming units (CFU) were counted and the total quantity of CFU was calculated.

Statistical Analysis: The maxima of the Soret bands of all *m*-THPC^x spectra were height normalized according to concentration. The fluorescence band of *m*-THPC was normalized to 1 and *m*-THPC^{c1}, *m*-THPC^{c1&2}, and *m*-THPC^{c4} were adjusted according to concentration. The evaluation of the washing experiments and the phototoxicity measurements was carried out by calculating mean ± standard error. The sample size for washing experiments was *n* = 3 and for the phototoxicity measurements with *E. coli* *n* = 16–54 and for *M. luteus* *n* = 6. A two-sample *t*-test was performed to show significant differences between nonirradiated and irradiated pairs for all chlorin coatings as well as for the nonmodified membranes. The significance level was 0.05, one-, and two-tailed *p*-values are substantially smaller than alpha values. Software for statistical analysis: Excel Analysis ToolPak Office 2019.

Supporting Information

Supporting Information is available from the Wiley Online Library or from the author.

Acknowledgements

The authors acknowledge M. Senge (Trinity College Dublin) for providing *m*-THPC, K. Skrodzky (Humboldt Universität zu Berlin) for the BET measurements, and K. Elsner (Humboldt Universität zu Berlin) for the SEM images. They also acknowledge the financial support for this work by the Deutsche Forschungsgemeinschaft (German Research Society BO 1762/12-1).

Open Access funding enabled and organized by Projekt DEAL.

Conflict of Interest

The authors declare no conflict of interest.

Data Availability Statement

The data that support the findings of this study are available from the corresponding author upon reasonable request.

Keywords

antibacterial coatings, light-activated reactive oxygen species (ROS) disinfection, membrane finish, microbial control of water filtration membranes, photodynamic therapy, singlet oxygen production

Received: September 7, 2022
Published online: October 6, 2022

- [1] a) C.-Y. Wang, P. Makvandi, E. N. Zare, F. R. Tay, L.-N. Niu, *Adv. Ther.* **2020**, *3*, 2000024; b) D. R. Monteiro, L. F. Gorup, A. S. Takamiya, A. C. Ruvolo-Filho, E. R. D. Camargo, D. B. Barbosa, *Int. J. Antimicrob. Agents* **2009**, *34*, 103.
- [2] a) V. B. Damodaran, N. S. Murthy, *Biomater. Res.* **2016**, *20*, 18; b) D. Davies, *Nat. Rev. Drug Discov.* **2003**, *2*, 114; c) K. M. Dobosz, K. W. Kolewe, J. D. Schiffman, *Front. Microbiol.* **2015**, *6*, 196.
- [3] a) S. L. Percival, L. Suleman, C. Vuotto, G. Donelli, *J. Med. Microbiol.* **2015**, *64*, 323; b) R. Gulati, S. Sharma, R. K. Sharma, *Polym. Bull.* **2021**; c) P. A. Fulmer, J. H. Wynne, *ACS Appl. Mater. Interfaces* **2011**, *3*, 2878; d) P. C. Sahoo, F. Kausar, J. H. Lee, J. I. Han, *RSC Adv.* **2014**, *4*, 32562.
- [4] Y. Parihar, E. Prasad **2020**, <https://www.alliedmarketresearch.com/anti-microbial-coatings-market-A07413> (accessed: September 2022).
- [5] a) U. Mahanta, M. Khandelwal, A. S. Deshpande, *J. Mater. Sci.* **2021**, *56*, 17915; b) B. Song, E. Zhang, X. Han, H. Zhu, Y. Shi, Z. Cao, *ACS Appl. Mater. Interfaces* **2020**, *12*, 21330.
- [6] a) H. Yazici, M. B. O'Neill, T. Kacar, B. R. Wilson, E. E. Oren, M. Sarikaya, C. Tamerler, *ACS Appl. Mater. Interfaces* **2016**, *8*, 5070; b) J. C. Tiller, C. Sprich, L. Hartmann, *J. Control. Release* **2005**, *103*, 355; c) K. Rapsch, F. F. Bier, M. Tadros, M. von Nickisch-Roseneck, *Bioconjugate Chem.* **2014**, *25*, 308; d) A. R. Statz, J. P. Park, N. P. Chongsirawatana, A. E. Barron, P. B. Messersmith, *Biofouling* **2008**, *24*, 439; e) A. Tiraferri, C. D. Vecitis, M. Elimelech, *ACS Appl. Mater. Interfaces* **2011**, *3*, 2869.
- [7] a) M. Li, L. Gao, C. Schlaich, J. Zhang, I. S. Donskyi, G. Yu, W. Li, Z. Tu, J. Rolff, T. Schwerdtle, R. Haag, N. Ma, *ACS Appl. Mater. Interfaces* **2017**, *9*, 35411; b) L. Dyshlyuk, O. Babich, S. Ivanova, N. Vasilchenko, V. Atuchin, I. Korolkov, D. Russakov, A. Prosekov, *Int. Biodeterior. Biodegrad.* **2020**, *146*, 104821; c) H. Ji, S. Zhou, Y. Fu, Y. Wang, J. Mi, T. Lu, X. Wang, C. Lü, *Mater. Sci. Eng., C* **2020**, *110*, 110735; d) J. Yin, Y. Yang, Z. Hu, B. Deng, *J. Membr. Sci.* **2013**, *441*, 73–82.
- [8] a) Z. Ferdous, A. Nemmar, *Int. J. Mol. Sci.* **2020**, *21*, 2375; b) G. V. Vimbela, S. M. Ngo, C. Frazee, L. Yang, D. A. Stout, *Int. J. Nanomed.* **2017**, *12*, 3941.
- [9] E. McCillicuddy, I. Murray, S. Kavanagh, L. Morrison, A. Fogarty, M. Cormican, P. Dockery, M. Prendergast, N. Rowan, D. Morris, *Sci. Total Environ.* **2017**, *575*, 231.
- [10] N. Niño-Martínez, M. F. Salas Orozco, G.-A. Martínez-Castañón, F. Torres Méndez, F. Ruiz, *Int. J. Mol. Sci.* **2019**, *20*, 2808.
- [11] a) C. Tanielian, C. Wolff, *J. Phys. Chem.* **1995**, *99*, 9825; b) S. Kimel, B. J. Tromberg, W. G. Roberts, M. W. Berns, *Photochem. Photobiol.* **1989**, *50*, 175–183.
- [12] T. J. Dougherty, C. J. Gomer, B. W. Henderson, G. Jori, D. Kessel, M. Korbelik, J. Moan, Q. Peng, *J. Natl. Cancer Inst. Monogr.* **1998**, *90*, 889.

- [13] R. M. Cordeiro, *Biochim. Biophys. Acta, Biomembr.* **2014**, 1838, 438.
- [14] M. Y. Memar, R. Ghotaslou, M. Samiei, K. Adibkia, *Infect. Drug Resist.* **2018**, 11, 567.
- [15] B. M. Amos-Tautua, S. P. Songca, O. S. Oluwafemi, *Molecules* **2019**, 24, 2456.
- [16] J. Li, W. Sun, Z. Yang, G. Gao, H.-H. Ran, K.-F. Xu, Q.-Y. Duan, X. Liu, F.-G. Wu, *ACS Appl. Mater. Interfaces* **2020**, 12, 54378.
- [17] a) S. S. Madaeni, *Water Res.* **1999**, 33, 301; b) D. S. Wavhal, E. R. Fisher, *J. Membr. Sci.* **2002**, 209, 255.
- [18] a) D. Kim, S. Jung, J. Sohn, H. Kim, S. Lee, *Desalination* **2009**, 238, 43; b) W. Yu, L. Xu, N. Graham, J. Qu, *Sci. Rep.* **2014**, 4, 6513; c) J. P. Chen, S. L. Kim, Y. P. Ting, *J. Membr. Sci.* **2003**, 219, 27.
- [19] A. Müller, A. Preuß, T. Bornhütter, I. Thomas, A. Prager, A. Schulze, B. Röder, *Photochem. Photobiol. Sci.* **2018**, 17, 1346.
- [20] M. O. Senge, J. C. Brandt, *Photochem. Photobiol.* **2011**, 87, 1240.
- [21] a) Q. Zhang, L. Fan, Z. Yang, R. Zhang, Y.-N. Liu, M. He, Y. Su, Z. Jiang, *App. Surf. Sci.* **2017**, 410, 494; b) S. L. Stanley, F. Scholle, J. Zhu, Y. Lu, X. Zhang, X. Situ, R. A. Ghiladi, *Nanomaterials* **2016**, 6, 77; c) B. L. Carpenter, F. Scholle, H. Sadeghifar, A. J. Francis, J. Boltersdorf, W. W. Wear, D. S. Argyropoulos, P. A. Maggard, R. A. Ghiladi, *Biomacromolecules* **2015**, 16, 2482; d) C. Ringot, N. Saad, F. Brégier, P. Bressollier, E. Poli, V. Chaleix, T. S. Ouk, V. Sol, *Photochem. Photobiol. Sci.* **2018**, 17, 1780; e) T. Wang, H. Ke, S. Chen, J. Wang, W. Yang, X. Cao, J. Liu, Q. Wei, R. A. Ghiladi, Q. Wang, *Mater. Sci. Eng., C* **2021**, 118, 111502; f) M. A. O. Sousa, M. A. C. de Faria, R. P. Ribeiro, J. V. P. Valverde, H. D. Rocha, K. F. dos Santos, M. S. Sousa, P. C. S. Souto, J. R. Silva, N. C. de Souza, *Photochem. Photobiol. Sci.* **2021**, 20, 1027; g) P. Kaner, D. J. Johnson, E. Seker, N. Hilal, S. A. Altinkaya, *J. Membr. Sci.* **2015**, 493, 807.
- [22] B. S. T. Peddinti, N. Morales-Gagnon, B. Pourdeyhimi, F. Scholle, R. J. Spontak, R. A. Ghiladi, *ACS Appl. Mater. Interfaces* **2021**, 13, 155.
- [23] B. S. T. Peddinti, F. Scholle, R. A. Ghiladi, R. J. Spontak, *ACS Appl. Mater. Interfaces* **2018**, 10, 25955.
- [24] a) J. Saiz-Poseu, J. Mancebo-Aracil, F. Nador, F. Busqué, D. Ruiz-Molina, *Angew. Chem., Int. Edit.* **2019**, 58, 696; b) P. Wilke, H. G. Börner, *ACS Macro Lett.* **2012**, 1, 871.
- [25] a) J. Horsch, P. Wilke, M. Pretzler, S. Seuss, I. Melnyk, A. Fery, A. Rempel, H. G. Börner, *Angew. Chem., Int. Edit.* **2018**, 57, 15728; b) P. Wilke, N. Helfricht, A. Mark, G. Papastavrou, D. Faivre, H. G. Börner, *J. Am. Chem. Soc.* **2014**, 136, 12667; c) J. M. Krüger, H. G. Börner, *Angew. Chem., Int. Ed.* **2021**, 60, 6408; d) S. Arias, S. Amini, J. Horsch, M. Pretzler, A. Rempel, I. Melnyk, D. Sychev, A. Fery, H. G. Börner, *Angew. Chem., Int. Ed.* **2020**, 59, 18495.
- [26] J. Saiz-Poseu, J. Mancebo-Aracil, F. Nador, F. Busqué, D. Ruiz-Molina, *Angew. Chem., Int. Edit.* **2019**, 58, 696.
- [27] M. Sun, Y. Su, C. Mu, Z. Jiang, *Ind. Eng. Chem. Res.* **2010**, 49, 790.
- [28] a) C. Lange, C. Lehmann, M. Mahler, P. J. Bednarski, *Cancers* **2019**, 11, 702; b) H. Anton, S. Bonneau, P. Maillard, K. Berg, D. Brault, *Photochem. Photobiol. Sci.* **2009**, 8, 778.
- [29] a) S. Wiczorek, E. Krause, S. Hackbarth, B. Röder, A. K. H. Hirsch, H. G. Börner, *J. Am. Chem. Soc.* **2013**, 135, 1711; b) Y. Liu, J. W. de Vries, Q. Liu, A. M. Hartmann, G. D. Wieland, S. Wiczorek, H. G. Börner, A. Wiehe, E. Buhler, M. C. A. Studart, W. R. Browne, A. Herrmann, A. K. H. Hirsch, *Chem. - Eur. J.* **2018**, 24, 798; c) F. Zabihi, S. Wiczorek, M. Dimd, S. Hedtrich, H. G. Börner, R. Haag, *J. Controlled Release* **2016**, 242, 35; d) S. Wiczorek, A. Dallmann, Z. Kochovski, H. G. Börner, *J. Am. Chem. Soc.* **2016**, 138, 9349; e) E. Maron, J. H. Swisher, J. J. Haven, T. Y. Meyer, T. Junkers, H. G. Börner, *Angew. Chem., Int. Ed.* **2019**, 58, 10747; f) S. Celasun, D. Remmler, T. Schwaar, M. G. Weller, F. Du Prez, H. G. Börner, *Angew. Chem., Int. Ed.* **2019**, 58, 1960.
- [30] a) M. Frigerio, M. Santagostino, *Tetrahedron Lett.* **1994**, 35, 8019; b) M. Pretzler, A. Bijelic, A. Rempel, *Sci. Rep.* **2017**, 7, 1810; c) J. Horsch, P. Wilke, H. Stephanowitz, E. Krause, H. G. Börner, *ACS Macro Lett.* **2019**, 8, 724; d) J. M. Krüger, C.-Y. Choi, P. Wang, O. Lösckke, D. Auhl, H. G. Börner, *Macromolecules* **2022**, 55, 989.
- [31] M. Saeed, M. Zahid, E. Rogan, E. Cavalieri, *Steroids* **2005**, 70, 173.
- [32] M. Gouterman, *J. Mol. Spectrosc.* **1961**, 6, 138.
- [33] R. Bonnett, B. D. Djelal, P. A. Hamilton, G. Martinez, F. Wierrani, *J. Photochem. Photobiol. B* **1999**, 53, 136.
- [34] M. Kress, T. Meier, R. Steiner, F. Dolp, R. Erdmann, U. Ortman, A. Rück, *J. Biomed. Opt.* **2003**, 8, 26.
- [35] S. Sasnouski, E. Pic, D. Dumas, V. Zorin, M. A. D'Hallewin, F. Guillemin, L. Bezdetsnaya, *Radiat. Res.* **2007**, 168, 209.
- [36] M. Regehly, E. A. Ermilov, M. Helmreich, A. Hirsch, N. Jux, B. Röder, *J. Phys. Chem. B* **2007**, 111, 998.
- [37] W. Choi, M. G. Shin, C. H. Yoo, H. Park, Y.-I. Park, J. S. Lee, J.-H. Lee, *J. Membr. Sci.* **2021**, 62615, 119212.
- [38] S. Krainer, U. Hirn, *Colloids Surf., A* **2021**, 619, 126503.
- [39] F. Cieplik, L. Tabenski, W. Buchalla, T. Maisch, *Front. Microbiol.* **2014**, 5, 405.
- [40] N. Vermeulen, W. J. Keeler, K. Nandakumar, K. T. Leung, *Biotechnol. Bioeng.* **2008**, 99, 550.
- [41] J. Pulit-Prociak, M. Banach, *Open Chem.* **2016**, 14, 76.
- [42] X. Gu, J. D. Jennings, J. Snarr, V. Chaudhary, J. E. Pollard, P. B. Savage, *Invest. Ophthalmol. Visual Sci.* **2013**, 54, 6217.
- [43] S. Zaccaria, R. C. van Gaal, M. Riool, S. A. J. Zaat, P. Y. W. Dankers, *J. Polym. Sci., Part A: Polym. Chem.* **2018**, 56, 1926.
- [44] D. K. Dimov, L. N. Gabriel, F. Lyon, C. R. Spain, P. D. Colburn, C. T. Schmidter, Z. Zhu, US20140017335A1, **2012**.